Radiative decay spectra of selected doubly excited states in helium

Johan Söderström,[1] Marcus Agåker,[1] Anna Zimina,[2] Raimund Feifel,[1] Stefan Eisebitt,[2] Rolf Follath,[2] Gerd Reichardt,[2] Olaf Schwarzkopf,[2] Wolfgang Eberhardt,[2] Andrej Mihelič,[3] Matjaž Žitnik,[3] and Jan-Erik Rubensson[1,2]

[1]*Physics Department, Uppsala Universitet, Box 530, S-751 21 Uppsala, Sweden*

[2]*BESSY, Albert-Einstein-Strasse 15 D-12489 Berlin, Germany*

[3]*Jožef Stefan Institute, Jamova cesta 39, SI-1000 Ljubljana, Slovenia*

(Received 13 June 2007; revised manuscript received 24 September 2007; published 28 January 2008)

Radiative decay spectra of doubly excited states in He have been measured after selective excitation with monochromatized synchrotron radiation. The decay spectra are in excellent agreement with predictions based on calculations.

DOI: 10.1103/PhysRevA.77.012513 PACS number(s): 32.30.−r, 31.15.A−, 32.50.+d, 32.80.−t

I. INTRODUCTION

Fluorescence from doubly excited states of helium was observed already in the 1920s [1], and high-resolution measurements were reported by Baltzer and Karlsson in the late 1980s [2]. Excitation spectra associated with these states were also recorded early on [3], and the measurement of the photoabsorption spectrum was one important early application of synchrotron radiation [4]. Technical advances during the later decades led to refined absorption spectra with a wealth of details [5]. The realization that the radiative decay channel is important for a detailed understanding of the photoabsorption spectrum [6–8] below the $N=2$ threshold has generated a lot of attention during recent years [9]. To characterize the excitation-emission scattering process, i.e., to determine the cross section for inelastic scattering to specific singly excited states, an experiment with high energy resolution both for exciting and scattered photons is called for. While the strongest transitions have been resolved earlier [10,11], most of the information about the decay paths has so far been inferred from measuring the long-wavelength fluorescence due to the further decay of the final states of the scattering process [10–13]. Theoretical predictions of the radiative decay rates have been presented [11,13–15], and especially the detailed pathways [15] have been derived for the interpretation of metastable atom [16] and fluorescence yield (FY) spectra [17].

Although there is a general qualitative agreement between indirectly determined branching ratios [10–13], and theoretical predictions [11,13–15], major quantitative deviations have been reported [11], and in details there are also obvious discrepancies in the results from different experimental investigations [13]. Here we present direct measurements of the branching ratios for population of singly excited final states after a selective excitation of doubly excited states below the $N=2$ threshold. We also present theoretical predictions which are in excellent quantitative agreement with the experimental results.

II. EXPERIMENT

The measurements were done at the U125/PGM-1 undulator beamline at BESSY-II [18]. The sample gas pressure was around 10 mbar in a closed cell with ultrathin Al filters ($\sim$1000 Å) allowing for transmission of the primary synchrotron radiation as well as secondary photons in the direction of a Rowland spectrometer (see Fig. 1). The spectrometer was operating with a grating of 2 m radius and 400 lines/mm, at an angle of incidence of 83.1°. The primary radiation was focused vertically into a 30-micron spot serving as a source for the spectrometer, which worked without an input slit. The spectrometer function was determined by recording the strong He II emission at 40.813 eV. Due to the large grating and the slitless operation this function is slightly asymmetric and has a full width at half-maximum (FWHM) of around 0.25 eV. The measured FWHM of the monochromator function was around 5 meV, and the energy scale was calibrated by shifting to literature values for the doubly excited states [5]. For the spectrometer energy scale we used the energy positions for the singly excited final states [19]. The spectrometer measured in the direction of polarization of the incoming beam with the acceptance angle being 36 mrad in the vertical and 87 mrad in the horizontal direction. In this geometry almost exclusively $n^a \rightarrow md$ [26] intensity is monitored [15]. In the dipole approximation the photon intensity is proportional to the geometric factor

$$f_l = \int d\Omega \left(1 + \frac{\beta_l}{4}(1 + 3P\cos 2\delta)\right), \tag{1}$$

which is determined by the final state selective asymmetry parameter β_l, the polarization of the incident radiation, P, the

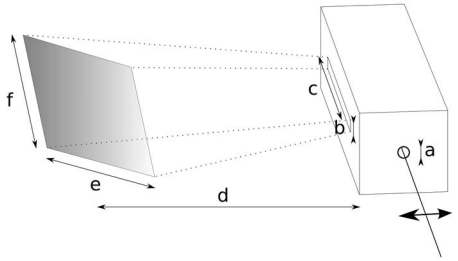

FIG. 1. Experimental geometry, $a=b=2$ mm, $c=15$ mm, the distance from the source to the spherical grating (shaded) is $d=235$ mm, and the active area on the grating is $e\times f=70\times 30$ mm^2. The grating is positioned in the direction of the polarization of the incoming radiation. After being diffracted at the grating the photons are detected by a multichannel plate detector positioned according to the Rowland condition.

angle between the polarization direction of the incident radiation and the propagation direction of the secondary photons, δ, and the acceptance solid angle of the spectrometer, Ω. Since $\beta_0=-1$ and $\beta_2=-1/10$ for *ms* and *md* final states, respectively, only $n^a \rightarrow md$ intensity would be expected if the acceptance angle is infinitely small and centered around $\delta=0$ and $P=1$. To simulate the actual experiment integration over the acceptance angle must be performed. Even if we allow for a possible misalignment of 2 degrees the integrand in (1) changes very little over the angular range and we can safely write the following:

$$\frac{f_0}{f_2} \approx \left(1-\frac{1}{4}(1+3P)\right) \Big/ \left(1-\frac{1}{40}(1+3P)\right). \tag{2}$$

The polarization is not measured in this experiment, but based on experience from similar beam lines we estimate that $P>0.98$. This sets the upper limit for the ratio between the geometrical factors, $f_0/f_2<0.02$. In the following, the theoretical analysis of the spectra will be based on the $n^a \rightarrow md$ scattering only.

III. THEORY

Two different theoretical approaches were employed to calculate the emission spectra. The first one relies on the standard multiconfiguration Hartree-Fock (MCHF) scheme to generate the wave functions and treats the absorption emission as a two-step process [15]. The lifetime broadening of the emission lines is much smaller than the spectrometer energy resolution, and the energy spread of the incoming photon beam does not allow a fully exclusive excitation of the resonance i centered at the energy ω_i, so that the emission spectrum measured at the energy of the scattered photon ω is in fact proportional to the cross section $d\sigma/d\omega$ convoluted with the spectrometer transmission function $T_\omega(\tilde{\omega})$ and the monochromator function $G_{\omega_0}(\tilde{\omega}_0)$,

$$\sigma^{\omega_i}(\omega) = \sum_j \int d\tilde{\omega}_0 G_{\omega_i}(\tilde{\omega}_0)\sigma_j \frac{(\Gamma_j+\gamma_j)/(2\pi)}{(\tilde{\omega}_0-\omega_j)^2+(\Gamma_j+\gamma_j)^2/4} \times \frac{\sum_f{}' \gamma_{jf}}{\Gamma_j+\gamma_j} T_\omega(E_g+\tilde{\omega}_0-E_f). \tag{3}$$

The total energy width of the intermediate state j is written as a sum of its autoionization width Γ_j and its total radiative width $\gamma_j=\Sigma_f\gamma_{jf}$, where γ_{jf} denotes the partial width for the transitions to the final state f. The widths Γ_j and γ_j, and the photoabsorption cross sections integrated over the energy of the incident photon [σ_j in Eq. (3)] are reported in Ref. [15]. The prime in Eq. (3) denotes that the summation runs only over the $1snd$ final states. The $j=i$ term yields a dominant contribution to the sum since the resonances under study are fairly well separated with respect to the energy width of the incoming photon beam. The asymmetric spectrometer response centered at the energy ω is represented by a sum of Gaussians (for its typical shape, see the 4^+ spectrum in Fig. 1). Note that the shape of $T_\omega(\tilde{\omega})$ was slightly different when the 3^0 and 4^0 spectra were recorded.

The second approach describes the absorption-emission process coherently within the second-order perturbation scheme, while the bound-continuum interaction is taken into account to all orders. The complex rotation method with a large Sturmian basis set (CRSB) is employed to improve the representation of intermediate doubly excited states [20,21]. The resulting eigenenergies match the previously presented reference values [22] to better than 0.14 meV, and are much more accurate than the corresponding MCHF values (Table I). We have calculated the cross section for inelastic photon scattering from the helium atom in its ground state g at the incoming photon energy ω_0, the scattered photon energy ω, and for the specific singly excited final state f. After integration over the full emission solid angle and summation over both polarizations, the cross section is expressed as

$$\frac{d\sigma_f^{\omega_0}}{d\omega} = \mathcal{M}_f^{\omega_0}(\omega)\,\delta(E_g+\omega_0-E_f-\omega), \tag{4}$$

where

$$\mathcal{M}_f^{\omega_0} = \frac{8\pi\alpha^4\omega^3\omega_0}{27}\left|\sum_j \frac{\langle\overline{\Psi_{f\theta}}\|D_\theta\|\Psi_{j\theta}\rangle\langle\overline{\Psi_{j\theta}}\|D_\theta\|\Psi_{g\theta}\rangle}{E_g+\omega_0-E_j+i(\Gamma_j+\gamma_j)/2}\right|^2. \tag{5}$$

The notation $\langle\overline{\Psi_\theta}\|D_\theta\|\Phi_\theta\rangle = e^{i\theta}\langle\overline{\Psi_\theta}\|D\|\Phi_\theta\rangle$ is used for reduced length-form of the matrix elements between complex-scaled states. The bar means that the deconjugated radial part of the wave function should be used in the evaluation of the radial integrals. The parameter θ denotes the "rotation angle," and α the fine structure constant. While the autoionization width Γ_j is simply proportional to the imaginary part of its complex energy eigenvalue and is obtained by diagonalizing the complex-scaled Hamiltonian, the radiative width γ_j of the resonance is estimated according to [20,21]

$$\gamma_j = \frac{4\alpha^3}{3(2L_j+1)}\sum_f (E_f-E_j)^3\,\mathrm{Re}\langle\overline{\Psi_{f\theta}}\|D_\theta\|\Psi_{j\theta}\rangle^2. \tag{6}$$

In Eq. (6), L_j is the total orbital momentum of the resonance state. The energy resolved emission spectrum measured at the nominal photon energy ω_i is then given by

$$\sigma^{\omega_i}(\omega) = \sum_f{}' \int d\tilde{\omega}_0 G_{\omega_i}(\tilde{\omega}_0)\mathcal{M}_f^{\tilde{\omega}_0}(E_g+\tilde{\omega}_0-E_f) \times T_\omega(E_g+\tilde{\omega}_0-E_f). \tag{7}$$

The branching ratio for the radiative transition between the resonance state i to the final state f can be defined as

$$b_{if} = \frac{\sigma_f^{\omega_i}}{\sum_f \sigma_f^{\omega_i}} = \frac{\mathcal{M}_f^{\omega_i}(E_g+\omega_i-E_f)}{\sum_f \mathcal{M}_f^{\omega_i}(E_g+\omega_i-E_f)}, \tag{8}$$

and can be directly compared to the result obtained from the MCHF calculations,

$$b_{if} = \frac{\gamma_{if}}{\sum_f \gamma_{if}}. \tag{9}$$

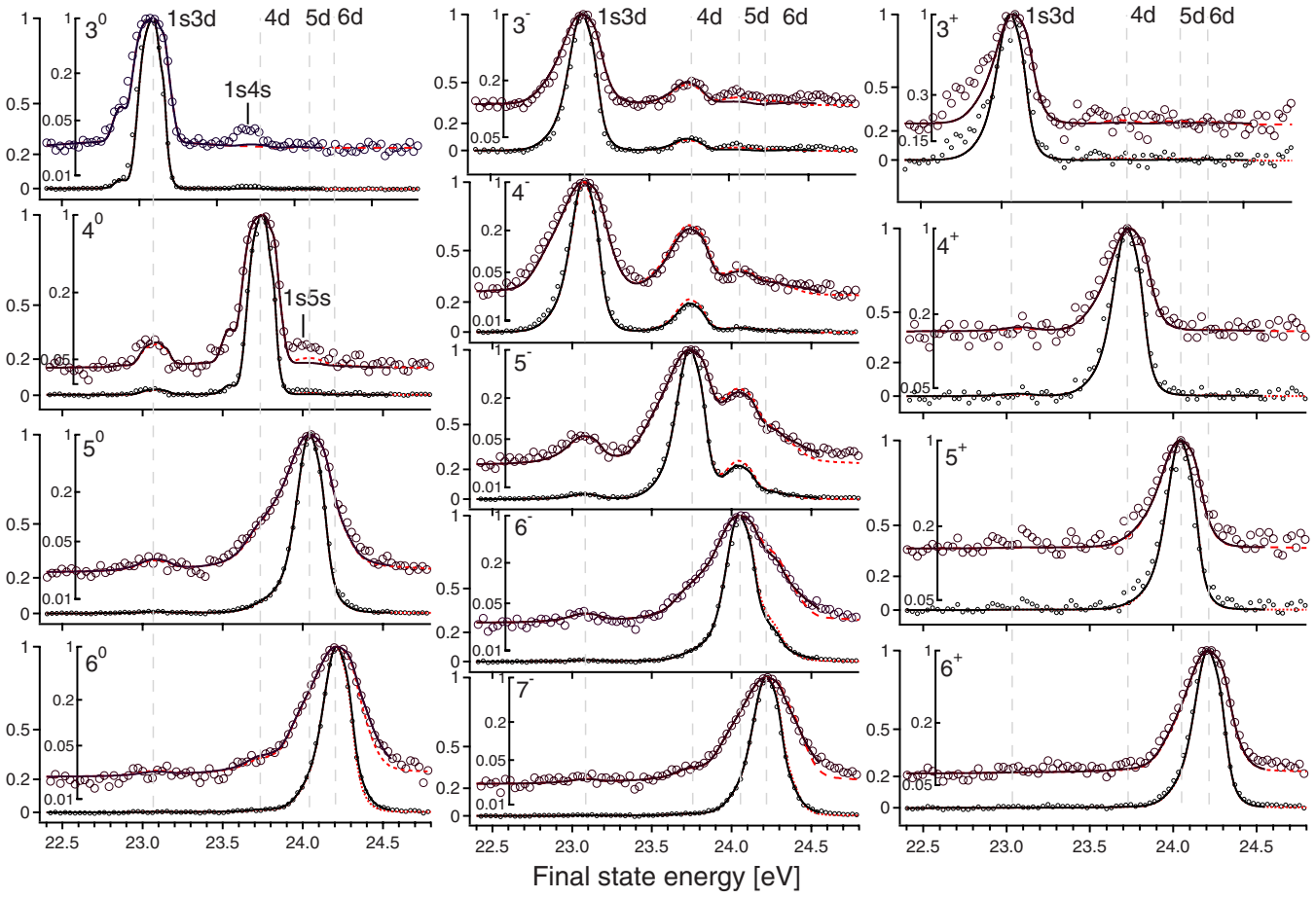

FIG. 2. (Color online) Experimental $n^{0,-,+} \rightarrow ml$ fluorescence spectra for $n=3-6$ (to $n=7$ for n^- resonances), where the intense 3^0 and 4^0 scattering is measured with better energy resolution than the other emission spectra presented above. The energy positions of the most prominent final states are marked with vertical dashed lines. The data are shown on both linear (outer) and logarithmic (inner) intensity scales. The curves through the data points are the normalized theoretical predictions $\sigma^{\omega_i}(\omega)$ of the CRSB (solid line) and MCHF (dotted, red) models. The length and velocity form plots of the latter do not differ on these graphs.

Both models predict specific dependence of the partial fluorescence yield integrated over the emission energies (PFY) as a function of the incoming photon energy. According to the MCHF model, the PFY is proportional to

$$\sigma(\omega_0) = \sum_j \sigma_j \sum_f{}' \gamma_{if} \int \frac{d\tilde{\omega}_0 G_{\omega_0}(\tilde{\omega}_0)/(2\pi)}{(\tilde{\omega}_0 - \omega_j)^2 + (\Gamma_j + \gamma_j)^2/4}. \quad (10)$$

The corresponding quantity of the CRSB model is given by

$$\sigma(\omega_0) = \sum_f{}' \int d\tilde{\omega}_0 G_{\omega_0}(\tilde{\omega}_0) \mathcal{M}_f^{\tilde{\omega}_0}(E_g + \tilde{\omega}_0 - E_f). \quad (11)$$

IV. RESULTS

Decay spectra excited at various resonances are shown in Fig. 2: For each incident photon energy, the photon yields (with the peak-value normalized to unity) are plotted versus the energy of the final state. The lines through the data points are intensity predictions from Eqs. (3) and (7) based on the two theories. The theory is normalized to give the best fit to each experimental spectrum.

Final states of $^1D_2$ symmetry are emphasized in the experimental geometry, and the results demonstrate that the "spectator" transition $n=m$ dominates for both $n^+ \rightarrow md$ and $n^0 \rightarrow md$ decay. For $n^- \rightarrow md$ decay, final states $m=n-1$ are populated most probably, with appreciable intensity found also for $m=n$. Qualitatively, this is in accordance with earlier direct measurements [10,11], and indirectly determined branching ratios [10–13]. Relative intensity determinations are straightforward in the direct measurements as the transitions occur within a small energy range so that the theoretical and experimental results can be compared with high accuracy over a large range of intensities.

Noticeable discrepancies between experiment and predictions are found in the n^0 decay spectra (see Fig. 2), where intensity for population of $1sns$ final states is observed ($3^0 \rightarrow 4s$ and $4^0 \rightarrow 5s$). Even with reasonable error estimates regarding polarization and alignment, the theory does not predict any significant $n^0 \rightarrow ms$ intensity. We tentatively attribute the observed intensity to exchange of angular momentum in collisions of the excited species, which tend to randomize the alignment created by the linearly polarized exciting radiation. This effect could be due to the high target pressure in

TABLE I. The resonance energies E_i (assuming infinitely heavy nucleus), the total inelastic photon scattering cross sections integrated over the incident photon energy in the region of the ith resonance ($\mathcal{F}_i$, see text), and branching ratios for the fluorescence decay b_{if} into 1*snd* and 1*sns* final states: (*o*) the MCHF [15], and (*n*) the CRSB [20] theory. The letters *l* and *v* denote the length and velocity form of the dipole transition matrix element, respectively. The number is omitted if $b_{if}<0.1\%$. Reported are also the results (*m*) derived from a previous experiment [11].

		$\mathcal{F}_i$	b_{if} (%)														
i	$-E_i$ (a.u.)	(barn×eV)	3*d*	4*d*	5*d*	6*d*	7*d*	8*d*	1*s*	2*s*	3*s*	4*s*	5*s*	6*s*	7*s*	8*s*	Type
3^0	0.5470898	269	79.3	0.1						6.2	2.9	9.2	1.3	0.5	0.2	0.1	*nl*
	0.54687	258	82.2							4.2	2.7	9.0	1.2	0.4	0.2	0.1	*ol*
		30.8	82.1							5.6	2.2	8.2	1.1	0.4	0.2	0.1	*ov*
		240	76.5	0.2	a	a	a	a	b	b	5.0	16.1	1.6	0.5	a	a	*m*
4^0	0.5276146	118	2.3	81.1	0.1					2.4	1.4	2.3	8.0	1.2	0.5	0.2	*nl*
	0.52750	190	2.1	82.3	0.5					1.5	1.2	2.4	8.0	1.1	0.4	0.2	*ol*
		5.9	2.6	82.1	0.3					2.2	1.2	2.0	7.7	1.1	0.4	0.2	*ov*
		142	6.3	79.6	a	1.5	a	a	b	b	2.4	1.8	8.4	a	a	a	*m*
5^0	0.5181172	63.4	0.6	2.7	81.6	0.7				1.2	0.7	0.7	2.5	7.2	1.1	0.4	*nl*
	0.51806	118	0.5	2.6	81.3	1.3	0.1			0.8	0.5	0.7	3.0	7.5	1.1	0.4	*ol*
		3.2	0.7	3.0	81.2	1.0				1.2	0.6	0.7	2.5	7.4	1.1	0.4	*ov*
		114	8.2	7.1	70.5	a	a	a	b	b	a	1.5	4.8	7.8	a	a	*m*
6^0	0.5127904	38.1	0.3	0.8	2.8	81.5	1.3	0.1	0.1	0.7	0.4	0.3	0.5	2.7	6.5	1.0	*nl*
	0.51276	70.1	0.2	0.7	2.8	80.2	1.8	0.2		0.5	0.3	0.4	0.6	3.7	7.5	1.1	*ol*
		3.1	0.3	0.9	3.0	80.0	1.6	0.2		0.7	0.4	0.4	0.6	3.4	7.5	1.1	*ov*
7^0	0.5095080	24.5	0.2	0.4	0.8	2.8	81.2	1.9	0.1	0.4	0.2	0.2	0.2	0.4	3.0	6.0	*nl*
	0.50950	40.1	0.1	0.3	0.8	2.9	79.6	2.3		0.3	0.2	0.2	0.3	0.6	4.7	7.6	*ol*
		3.5	0.2	0.4	0.9	3.0	79.1	2.1		0.5	0.3	0.2	0.3	0.6	4.6	7.9	*ov*
3^-	0.5970738	121	9.6	0.8	0.2	0.1	0.1		0.1	54.8	29.1	3.0	0.9	0.4	0.2	0.1	*nl*
	0.59661	66.0	7.8	0.6	0.2					54.9	31.3	3.2	1.0	0.5	0.3	0.2	*ol*
		123	10.0	0.9	0.3	0.1				55.0	28.9	2.9	0.9	0.4	0.2	0.1	*ov*
4^-	0.5464919	105	46.5	8.5	1.1	0.3	0.2	0.1		2.1	23.1	14.9	1.7	0.6	0.3	0.2	*nl*
	0.54625	136	42.8	9.3	1.1	0.4	0.2			2.9	22.7	17.5	2.0	0.7	0.3	0.2	*ol*
		133	43.0	9.6	1.2	0.4	0.2	0.1		2.7	23.4	16.5	1.9	0.6	0.3	0.2	*ov*
		109	38.8	9.8	0.8	0.4	a	a	b	b	33.3	15.3	1.2	0.4	a	a	*m*
5^-	0.5272970	95.8	1.4	43.5	9.1	1.3	0.5	0.2		0.9	1.6	22.4	15.2	1.9	0.7	0.3	*nl*
	0.52717	142	1.3	41.7	10.1	1.4	0.5	0.2		1.1	1.6	21.6	17.2	2.1	0.7	0.4	*ol*
		131	1.4	41.7	10.2	1.5	0.5	0.3		1.1	1.7	22.0	16.6	2.0	0.7	0.3	*ov*
		106	5.2	46.0	8.4	0.8	a	a	b	b	2.0	21.0	14.5	2.0	a	a	*m*
6^-	0.5179369	84.1	0.4	1.7	42.7	9.0	1.4	0.5		0.5	0.5	1.7	22.4	14.9	1.9	0.7	*nl*
	0.51787	133	0.3	1.7	42.2	10.2	1.6	0.6		0.6	0.5	1.6	21.5	16.5	2.1	0.7	*ol*
		119	0.4	1.8	42.2	10.2	1.6	0.6		0.5	0.5	1.7	21.7	16.1	2.0	0.7	*ov*
		138	4.6	4.9	42.4	5.9	1.5	a	b	b	a	2.2	20.1	13.3	4.9	a	*m*
7^-	0.5126797	71.3	0.1	0.5	1.8	42.6	8.8	1.5		0.3	0.2	0.5	1.8	22.5	14.6	1.9	*nl*
	0.51264	123	0.1	0.5	1.9	43.7	10.2	1.6		0.3	0.2	0.5	1.7	21.4	15.7	2.0	*ol*
		107	0.2	0.5	2.0	43.6	10.1	1.6		0.3	0.3	0.6	1.8	21.6	15.5	2.0	*ov*
3^+	0.5640803	70.2	18.9	0.3	0.3	0.3	0.3	0.3	1.5	0.3	72.7	0.8	0.3	0.2	0.2	0.1	*nl*
	0.56298	82.5	20.0	0.3	0.2	0.1			0.9	0.4	77.3	0.4	0.1				*ol*
		63.5	20.2	0.2	0.2				0.7	0.3	77.6	0.5	0.1				*ov*
		98	15.1	12.8	a	a	a	a	b	b	60.4	11.6	a	a	a	a	*m*
4^+	0.5343612	68.0	0.4	23.0	0.1	0.1	0.1	0.1	0.7		0.6	72.5	0.5	0.2	0.1	0.1	*nl*
	0.53390	81.0	0.2	23.4					0.3		0.4	75.3	0.2				*ol*
		62.5	0.2	23.4					0.3		0.4	75.5	0.2				*ov*
		99	a	29.2	a	a	a	a	b	b	a	70.7	a	a	a	a	*m*

TABLE I. (*Continued.*)

		$\mathcal{F}_i$	b_{if} (%)													
i	$-E_i$ (a.u.)	(barn×eV)	$3d$	$4d$	$5d$	$6d$	$7d$	$8d$	$1s$	$2s$	$3s$	$4s$	$5s$	$6s$	$7s$	$8s$	Type
5^+	0.5215037	67.5	0.1	0.4	24.4	0.1			0.3		0.1	0.4	72.6	0.3	0.1	0.1	*nl*
	0.52128	80.5		0.2	24.5				0.2			0.3	74.6				*ol*
		62.1		0.2	24.3				0.1			0.2	74.9	0.1			*ov*
		106	[a]	4.2	23.3	[a]	[a]	[a]	[b]	[b]	[a]	[a]	72.4	[a]	[a]	[a]	*m*
6^+	0.5147334	66.9		0.1	0.5	24.9	0.1		0.2			0.1	0.3	72.7	0.3	0.1	*nl*
	0.51461	80.5			0.2	24.7							0.1	74.6			*ol*
		62.0			0.2	24.6							0.1	74.7			*ov*
		84	[a]	[a]	3.6	21.4	[a]	[a]	[b]	[b]	[a]	[a]	1.8	73.2	[a]	[a]	*m*
7^+	0.5107264	66.7			0.1	0.5	25.2	0.2	0.1				0.1	0.3	72.7	0.2	*nl*
	0.51066	80.2				0.2	24.6	0.1						0.1	74.7		*ol*
		61.6				0.2	24.7	0.1							74.7		*ov*
		65	[a]	[a]	[a]	[a]	21.9	[a]	[b]	[b]	[a]	[a]	[a]	[a]	78.1	[a]	*m*

[a]Weak, not detected transitions.
[b]Not measured transitions.

combination with the relatively long lifetime of the n^0 states which is of the order of 0.2 ns [23]. In a crude hard-sphere approximation, the average time between collisions depends on the average velocity of atoms, their size and density. For helium gas at 10 mbar and at room temperature with radius of excited atoms set to 12 Bohr radii the collision time is around 400 ps. While this is comparable to the lifetimes of observed n^0 states, the n^- and n^+ states have substantially shorter lifetimes.

Within the dynamic range of the experiment, which allows for measurements of lines with less than 1% of the intensity of the strongest lines, we see that both theories predict the results very well. Quantitatively, this result is at variance with earlier findings, e.g., a large deviation between theory and experiment regarding the intensity of the $n^- \rightarrow (n-2)d$ which has earlier been inferred [11], whereas the agreement here is very good. In details we see that the CRSB theory is in better agreement with the experimental result than the MCHF theory. Notably, the MCHF prediction of the intensity ratio between the two strongest lines in the n^- emission spectra differs significantly from the experimental result, whereas no such deviation is found for the CSRB prediction. Apart from the $n^a \rightarrow ms$ contamination described above we do not find any significant discrepancies between the experiment and the theory.

This demonstrates that the decay spectra, reflecting the relative radiative branching ratios, are highly sensitive to the description of the doubly excited states, and that the CRSB results represent a refinement with respect to the MCHF model. In Table I, the calculated branching ratios b_{if} both for *ms* and *md* final states are shown for each intermediate state. For comparison we also report branching ratios extracted from the previously measured cross sections (Table I of [11]), except for the 3^- state where the extraction procedure yields an unreliable result due to the relatively strong but unobserved transitions to $1s$ and $2s$ final states. In principle, transition to these final states occur also for the other resonances but according to the calculations their intensity is expected to be 5% (for 3^0 state) or less of the total fluorescence intensity.

Since the natural energy width of the resonances is small in comparison to the energy differences between the resonances, we could further compare both theories: the CSRB total fluorescence cross section of each resonance i could be estimated by integrating the partial fluorescence yield [equal to Eq. (11) without the prime in the summation] across the resonance. In Table I this is compared to the total fluorescence cross section $\mathcal{F}_i = \sigma_i \gamma_i / (\Gamma_i + \gamma_i)$ in the length and velocity form, as given in the framework of the MCHF model. Taking into account a proper apparatus function (Gaussian with $\Gamma_{\text{app}} = 4$ meV) the total fluorescence cross-section values were also deduced from the experimental cross sections [11], which correspond to the maxima of the resonance profiles.

Partial fluorescence yield spectra, where the total count rate of the spectrometer in the 38–42 eV emission energy range is measured as a function of excitation energy, under the same experimental conditions as before, are shown in Fig. 3. The relative spectral intensities are similar to what is seen in less selective fluorescence yield spectra [17,24], and the measured data allow to test thoroughly the predictions of both theories regarding the relative strength of partial fluorescence signal pertaining to $n^0, (n+1)^-$ doublets with $n=3-5$. The agreement with theoretical predictions (10) and (11) is again very good but we note that also here, in the "integrated mode," the CRSB theory does slightly better than MCHF in the length form. This remains true even if 1%–2% correction on the n^0 intensity is applied due to the observed transitions to $1sns$ final states. With the present experimental data quality, we do not find any significant disagreement with the theoretical predictions. Remarkably, the PFY in the velocity form is far off the experimental result due to the strong underestimation of the total fluorescence cross section of n^0 states (Table I). Although the branching ratios for radiative decay in the velocity form are close to the length form result, the photoabsorption cross section of the diffuse n^0 states is

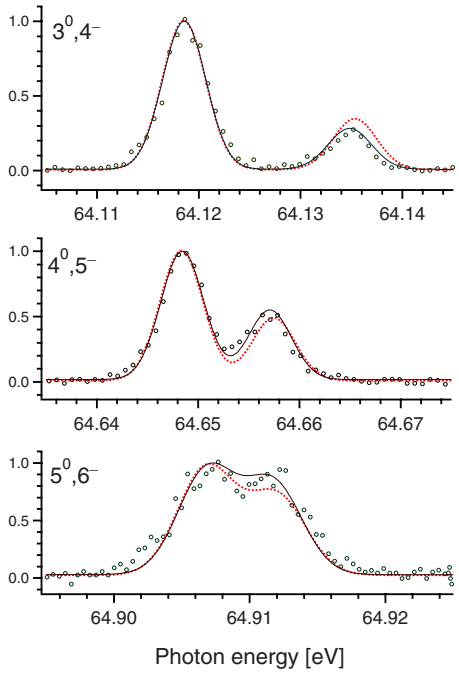

FIG. 3. (Color online) Partial (~38–42 eV) FY spectra of $n^0,(n+1)^-$ doublets in experimental geometry which emphasizes $^1D_2$ final states. The data is compared with $\sigma(\omega_0)$ of the CRSB (solid line) and of the MCHF model in the length form (dotted, red). The theory is scaled down to match the signal of the n^0 resonance. The MCHF result was shifted toward lower energy (see Table I).

not calculated reliably in the MCHF velocity form. As the velocity form relies more on the accurate description of an inner part of the wave function than the length form, it follows that MCHF better describes the outer region of these states.

Further measurements of that kind are needed and they should extend over the larger incoming photon energy interval to test the PFY shape and relative intensity for a larger number of resonances. One should be aware that the shape of the energy resolved emission spectrum which is acquired at fixed nominal incoming photon energy is less sensitive to the precise experimental conditions, but the shape of PFY spectrum can strongly depend on the gas cell pressure and temperature. Since high resolution experiments tend to employ the pressure in the mbar range to obtain sufficient photon intensity, a self-absorption correction is needed prior to comparing the theoretical single atom cross sections to the measured data. At present perpendicular experimental geometry, the correction factor for $\sigma(\omega_0)$ is given by $\{1-\exp[\mu(\omega_0)L]\}/[\mu(\omega_0)L]$, where L is the length of the gas cell [25]. The absorption coefficient μ is proportional to the Doppler broadened single atom photoabsorption cross section $\sigma^A(\omega_0)\approx\sigma^I(\omega_0)+\sigma(\omega_0)$. To estimate the latter we have calculated photoionization cross section $\sigma^I(\omega)$ with our complex rotated states, applying the standard procedure [21]. The correction factor was calculated for 10 mm of gas at 10 mbar pressure and at room temperature, and the convolution with the incoming photon beam energy profile was done, similar to (11), but considering also the energy-dependent correction factor. In our case the resulting PFY profiles are predicted to differ substantially from the zero pressure limit only for n^+ resonances, where target absorption varies the most. It is estimated that the calculated single atom PFY signal is dumped by 50% for the 3^+ resonance due to the enhanced photon absorption in the gas cell. The PFY line shape of the n^+ states is affected, too, and assumes an asymmetric shape which mirrors the shape of the corresponding photoabsorption line. This effect cannot be verified by the present experiment because the statistical uncertainty of the data is too high.

V. CONCLUSIONS

In conclusion, we have presented selectively excited fluorescence spectra of the lowest helium double excitations, and compared the results to theoretical results. The predictions and the experimental results are in excellent agreement. For the radiative branching ratios for populating 1*snd* final states, the comparison between experiment and theory could be done at a high level of accuracy. Theoretical predictions are also in agreement with the measured partial fluorescence yield spectra.

ACKNOWLEDGMENTS

The authors gratefully acknowledge the support from the Swedish Research Council, the Swedish Foundation for Strategic Research, the Göran Gustafsson Foundation, and the Slovenian Ministry of Higher Education, Science, and Technology (research program P1-0112). The authors are grateful for the support by the BESSY staff.

[1] K. T. Compton and J. C. Boyce, J. Franklin Inst. **205**, 497 (1928).
[2] P. Baltzer and L. Karlsson, Phys. Rev. A **38**, 2322 (1988).
[3] R. Whiddington and H. Priestley, Proc. R. Soc. London, Ser. A **145**, 462 (1934).
[4] R. P. Madden and K. Codling, Phys. Rev. Lett. **10**, 516 (1963).
[5] K. Schulz, G. Kaindl, M. Domke, J. D. Bozek, P. A. Heimann, A. S. Schlachter, and J.-M. Rost, Phys. Rev. Lett. **77**, 3086 (1996).
[6] M. K. Odling-Smee, E. Sokell, P. Hammond, and M. A. MacDonald, Phys. Rev. Lett. **84**, 2598 (2000).
[7] J.-E. Rubensson, C. Såthe, S. Cramm, B. Kessler, S. Stranges, R. Richter, M. Alagia, and M. Coreno, Phys. Rev. Lett. **83**, 947 (1999).
[8] T. W. Gorczyca, J.-E. Rubensson, C. Såthe, M. Ström, M. Agåker, D. Ding, S. Stranges, R. Richter, and M. Alagia, Phys. Rev. Lett. **85**, 1202 (2000).
[9] See, e.g., P. Hammond, J. Electron Spectrosc. Relat. Phenom.

144–147, 13 (2005), and references therein.
[10] K.-H. Schartner, B. Zimmermann, S. Kammer, S. Mickat, H. Schmoranzer, A. Ehresmann, H. Liebel, R. Follath, and G. Reichardt, Phys. Rev. A **64**, 040501(R) (2001).
[11] S. Mickat, K.-H. Schartner, S. Kammer, R. Schill, L. Werner, S. Klumpp, A. Ehresmann, H. Schmoranzer, and V. L. Suhkhorukov, J. Phys. B **38**, 2613 (2005).
[12] M. Coreno, M. de Simone, M. Danailov, R. Richter, A. Kivimäki, M. Žitnik, and K. C. Prince, J. Electron Spectrosc. Relat. Phenom. **144–147**, 39 (2005).
[13] M. Coreno, K. C. Prince, R. Richter, M. de Simone, K. Bučar, and M. Žitnik, Phys. Rev. A **72**, 052512 (2005).
[14] C.-N. Liu, M.-K. Chen, and C. D. Lin, Phys. Rev. A **64**, 010501(R) (2001).
[15] M. Žitnik, K. Bučar, M. Štuhec, F. Penent, R. I. Hall, and P. Lablanquie, Phys. Rev. A **65**, 032520 (2002).
[16] J. G. Lambourne, F. Penent, P. Lablanquie, R. I. Hall, M. Ahmad, M. Žitnik, K. Bučar, P. Hammond, S. Stranges, R. Richter, M. Alagia, and M. Coreno, J. Phys. B **36**, 4339 (2003).
[17] J. G. Lambourne, F. Penent, P. Lablanquie, R. I. Hall, M. Ahmad, M. Žitnik, K. Bučar, P. Hammond, S. Stranges, R. Richter, M. Alagia, and M. Coreno, J. Phys. B **36**, 4351 (2003).
[18] R. Follath and F. Senf, Nucl. Instrum. Methods Phys. Res. A **390**, 388 (1997).
[19] NIST Atomic Spectra Database, http://physics.nist.gov/PhysRefData/ASD/index.html
[20] A. Mihelič, Ph.D. thesis, University of Ljubljana, 2006, http://www.rcp.ijs.si/amihelic/phd/thesis.pdf
[21] A. Mihelič and M. Žitnik, Phys. Rev. Lett. **98**, 243002 (2007).
[22] J.-M. Rost, K. Schulz, M. Domke, and G. Kaindl, J. Phys. B **30**, 4663 (1997).
[23] J. G. Lambourne, F. Penent, P. Lablanquie, R. I. Hall, M. Ahmad, M. Žitnik, K. Bučar, M. K. Odling-Smee, J. R. Harries, P. Hammond, D. K. Waterhouse, S. Stranges, R. Richter, M. Alagia, M. Coreno, and M. Ferianis, Phys. Rev. Lett. **90**, 153004 (2003).
[24] C. Såthe, M. Ström, M. Agåker, S. Stranges, R. Richter, M. Alagia, A. Mihelič, M. Žitnik, and J. E. Rubensson (to be published).
[25] F. Gel'mukhanov and H. Ågren, Phys. Rep. **312**, 87 (1999).
[26] A simplified notation of the three dipole allowed series of doubly excited $^1P_1^o$ states is used, which originates in the first-order description of these states: $(2snp+2pns)$, $(2snp-2pns)$, and $2pnd$ states, respectively. The final states have $^1D_2^e$ or $^1S_0^e$ symmetry and they are singly excited so that the scattering path (neglecting interference) can be unambiguously referred to as $n^a \rightarrow ml$, where m is the principal quantum number, $a = \pm, 0$, and $l = s, d$.